LETTERS

Helical extension of the neuronal SNARE complex into the membrane

Alexander Stein[1], Gert Weber[2,3], Markus C. Wahl[2,3] & Reinhard Jahn[1]

Neurotransmission relies on synaptic vesicles fusing with the membrane of nerve cells to release their neurotransmitter content into the synaptic cleft, a process requiring the assembly of several members of the SNARE (soluble *N*-ethylmaleimide-sensitive factor attachment protein receptor) family. SNAREs represent an evolutionarily conserved protein family that mediates membrane fusion in the secretory and endocytic pathways of eukaryotic cells[1–3]. On membrane contact, these proteins assemble *in trans* between the membranes as a bundle of four α-helices, with the energy released during assembly being thought to drive fusion[4–6]. However, it is unclear how the energy is transferred to the membranes and whether assembly is conformationally linked to fusion. Here, we report the X-ray structure of the neuronal SNARE complex, consisting of rat syntaxin 1A, SNAP-25 and synaptobrevin 2, with the carboxy-terminal linkers and transmembrane regions at 3.4 Å resolution. The structure shows that assembly proceeds beyond the already known core SNARE complex[7], resulting in a continuous helical bundle that is further stabilized by side-chain interactions in the linker region. Our results suggest that the final phase of SNARE assembly is directly coupled to membrane merger.

SNAREs are characterized by conserved stretches of 60–70 amino acids termed SNARE motifs[2,8,9]. In syntaxin 1A and synaptobrevin 2, the SNARE motifs are connected by short linkers to C-terminal transmembrane regions (TMRs) (Fig. 1a). SNAP-25 is anchored to the plasma membrane by means of palmitoyl chains bound to cysteine residues in a loop region connecting its two SNARE motifs. SNARE motifs are largely unstructured, but spontaneously assemble into helical SNARE complexes[10,11]. The X-ray structure of the synaptic core complex, which is paradigmatic for all other SNARE complexes studied so far, revealed four intertwined, parallel α-helices, with each helix being provided by a different SNARE motif. The centre of the bundle contains 16 stacked layers of interacting, mostly hydrophobic side chains[7].

Assembly of SNARE complexes is initiated amino-terminally and proceeds towards the C terminus in a zipper-like fashion, thus pulling the membranes together[12,13]. However, it is unclear whether zippering extends all the way into the membrane or whether the linkers between the helical SNARE motifs and the transmembrane regions remain free and flexible, with the final step in membrane merger being effected by other factors[14–17].

First, we tested whether the linkers and TMRs add stability to the neuronal SNARE complex. Whereas the core complex containing only the SNARE motifs is already known to be very stable[18], the complex including linkers and TMRs of both syntaxin 1 and synaptobrevin 2 was significantly more resistant to thermal and chemical denaturation than the core complex alone (Fig. 1b, c). When only the TMR of syntaxin 1A was present, resistance to thermal and chemical denaturation approximated that of the core complex. When only the

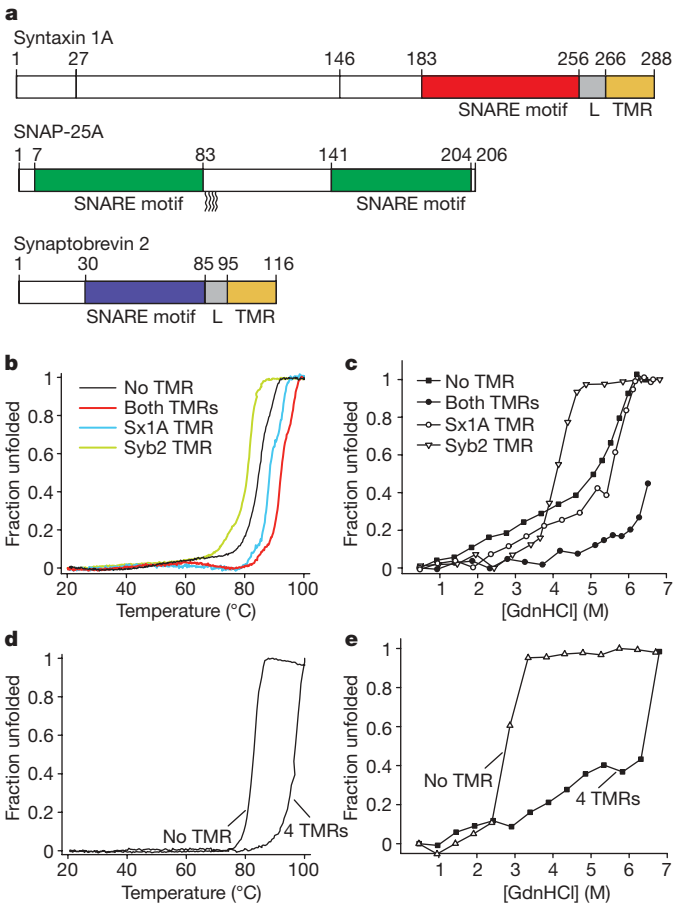

Figure 1 | Linkers and transmembrane regions add stability to SNARE complexes. a, Protein fragments used in this study. The complex used for crystallization contained all coloured segments. For circular dichroism (CD) measurements, complexes were formed with the same syntaxin 1A fragment, but with full-length synaptobrevin 2 and SNAP-25a (all cysteines replaced by serines). **b**–**e**, Unfolding of SNARE complexes, monitored by CD spectroscopy at 222 nm. **b**, Thermal unfolding of synaptic SNARE complexes in which the TMRs were either present or in which one or both of the TMRs were lacking. Note that the complex used for crystallization unfolded at approximately 97 °C (see Table 1). Sx1a, syntaxin 1A; Syb2, synaptobrevin 2. **c**, Unfolding of the same complexes at increasing concentrations of guanidine hydrochloride (GdnHCl). **d**, Thermal unfolding of endosomal SNARE complexes consisting of syntaxin 7, syntaxin 8, Vti1b and endobrevin, either containing or lacking its four TMRs. **e**, Unfolding of the endosomal complexes at increasing concentrations of GdnHCl.

[1]Department of Neurobiology, [2]Research Group X-ray Crystallography, Max Planck Institute for Biophysical Chemistry, 37077 Göttingen, Germany. [3]Freie Universität Berlin, Fachbereich Biologie, Chemie, Pharmazie, Institut für Chemie und Biochemie, AG Strukturbiochemie, Takustraße 6, D-14195 Berlin, Germany.

TMR of synaptobrevin 2 was present, stability was lower than that of the core complex, suggesting that the presence of the free C-terminal portion of synaptobrevin interferes with the packing of the four-helix bundle further upstream. Similarly, an endosomal SNARE complex that was composed of syntaxin 7, syntaxin 8, Vti1b and endobrevin and that contained all four TMRs was more stable than the corresponding core complex (Fig. 1d, e). These findings are in agreement with an earlier study reporting increased thermal stability of the SDS-resistant band pattern in SDS–polyacrylamide gel electrophoresis and protection of the linker region from trypsin digestion, and suggest that stabilizing interactions between SNAREs extend into the linker and TMRs[19].

Second, to obtain structural information about the crucial C-terminal region, we solved the X-ray structure of a neuronal SNARE complex that included the TMRs of syntaxin 1A and synaptobrevin 2. Using *n*-nonyl β-D-glucopyranoside as detergent, we obtained crystals of space group *C*2 that diffracted to 3.4 Å. To solve the structure, initial experimental phases were obtained by single-wavelength anomalous dispersion (SAD) phasing using a complex with selenomethionine-labelled syntaxin 1A, which was crystallized and diffracted to a resolution of 4.3 Å (see Supplementary Fig. 1a–c for densities obtained by SAD phasing and Supplementary Fig. 2a, b for final $2F_o-F_c$ maps).

As previously seen in the structure of the core complex[7], the four SNARE motifs form a four-helix bundle. The most striking feature is that both syntaxin 1A and synaptobrevin 2 form continuous helices throughout their SNARE motifs, linker regions and TMRs (see Fig. 2a for an overview, Fig. 2b for an electrostatic surface plot, Fig. 2c for a close-up view on the linkers and TMRs, and Fig. 2d for a schematic representation of the interacting amino acids). In the crystal, hydrophobic contacts between the TMRs of synaptobrevin 2 and syntaxin 1A mediate the association of four complexes through their TMRs, forming an X-shaped assembly. Four synaptobrevin 2 TMRs build the core of this complex, surrounded by four TMRs from syntaxin 1A (Supplementary Fig. 3a).

The two complexes in an asymmetric unit are very similar (root mean squared deviation (r.m.s.d.) = 0.6 Å). The structures of the four-helical core of the complex closely resemble the previously published structures (r.m.s.d. = 0.90 and 0.82 Å compared with the structure in ref. 20, except for the last layer (+8), which is not completely resolved). The linker region contains a collar of aromatic residues that is surrounded predominantly by basic residues (Fig. 3). Tyr 257 is part of this layer and is deeply buried in a pocket formed by three flanking lysine residues of syntaxin 1A (Lys 253, Lys 256 and Lys 260) and four residues of synaptobrevin 2 (Lys 85, Arg 86, Trp 89 and Asn 92). In addition, Lys 264 of syntaxin 1A engages in a hydrogen bond with Asn 92 of synaptobrevin 2. To investigate the importance of amino acid contacts in the linker region, we mutated several residues of syntaxin 1A to alanines (which are readily accommodated in α-helices) and subjected the corresponding complexes to thermal unfolding. Only substitution of Tyr 257 resulted in reduced thermal stability, whereas the effects of the other mutations on the melting transition temperature were not significant (Table 1). Apparently, intermolecular side-chain contacts in the aromatic layer are crucial for stability and may stiffen the linker region.

Considerable electron density is observed around the linker regions, which cannot be ascribed to protein residues, but rather seems to result from sulphate ions, glycylglycylglycine and *n*-nonyl β-D-glucopyranoside molecules in the crystallization buffer. Although owing to the limited resolution the positions of glycylglycylglycine and *n*-nonyl β-D-glucopyranoside are uncertain, the sulphate ions are in contact with multiple positively charged side chains. In a biological membrane, these basic residues would probably be stabilized by lipid head-groups. Indeed, the polybasic region in syntaxin 1A is known to interact with negatively charged lipids.

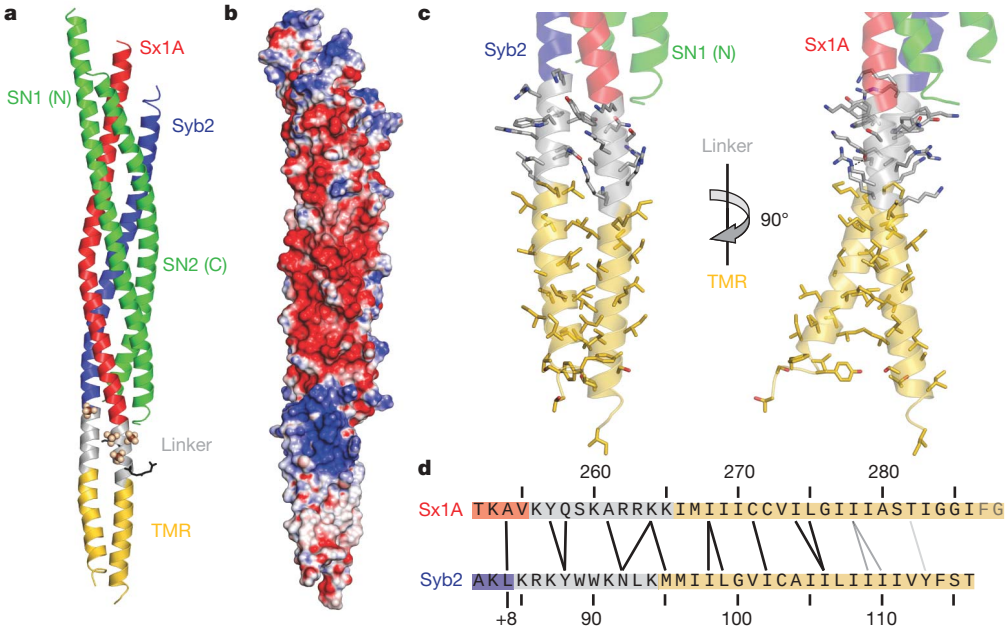

Figure 2 | Synaptobrevin 2 and syntaxin 1A form continuous helices. **a**, Ribbon plot of the synaptic SNARE complex including linkers and TMRs (colour coding as in Fig. 1a). Sulphate ions and two glycylglycylglycine molecules are depicted as spheres and black sticks, respectively. **b**, Surface plot showing the electrostatic potential of the synaptic SNARE complex (blue, positive charge; red, negative charge). The electrostatic surface was contoured between –16 and +16 kT e^{-1}. **c**, Ribbon plot showing linkers and TMRs of synaptobrevin 2 and syntaxin 1A. Side chains are shown as sticks, with carbons coloured as the corresponding backbone; oxygen, red; nitrogen, blue. The hydrogen bond between Asn 92 in synaptobrevin 2 and Lys 264 in syntaxin 1A is depicted as a black dashed line. The right panel is rotated by 90° about the vertical axis as indicated. **d**, Amino acids forming interactions between the two linkers and TMRs. Amino acids that are close to each other are connected by black lines, those further away but facing towards each other by grey lines. The last two amino acids in syntaxin 1A were not resolved in the structure. +8 indicates the C-terminal layer of the four-helix bundle[27]. Note that this layer is not completely resolved as electron density for the last four amino acids of the second helix of SNAP-25 (including the layer-forming amino acid Met 202) is absent.

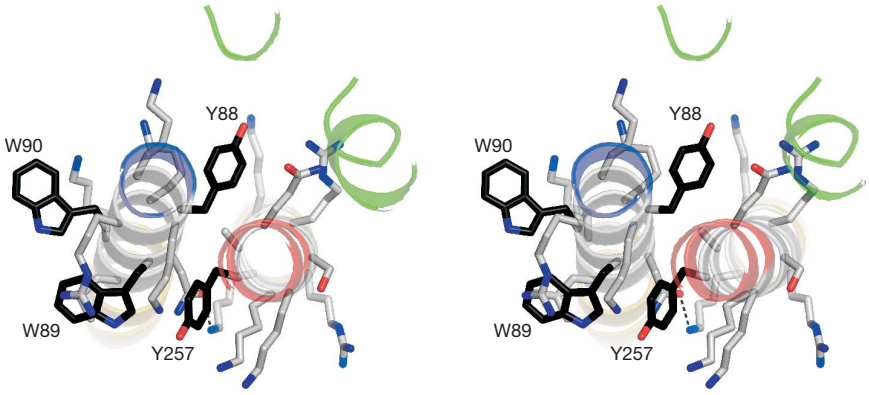

Figure 3 | An aromatic layer appears to be crucial for linker contact. Stereo view of the aromatic residues in the linker regions viewed from the N terminus. Carbon atoms in the side chains of aromatic amino acids are shown in black; otherwise, the same colour code as in Fig. 2 is used.

Mutation of these residues reduced the affinity for these lipids and resulted in a decrease in evoked secretion from bovine chromaffin cells[21].

C-terminally adjacent to the linker regions, the TMRs remain in contact, with residues Met 95, Ile 98, Leu 99, Ile 102 and Ile 106 in synaptobrevin 2, and Ile 268, Cys 271, Ile 274 and Leu 275 in syntaxin 1A largely contributing to the interaction surface. Beyond this region, the two TMRs veer away from each other. We also solved the structure of a complex purified and crystallized using *n*-heptyl β-D-glucopyranoside as a detergent. These crystals diffracted to 4.8 Å resolution, belong to space group $I2_12_12_1$, and again harbour two very similar complexes per asymmetric unit (see Supplementary Fig. 2c for the model overlaid on the $2F_o-F_c$ map). Although the overall structures of the complexes are very similar to the structures of the complexes in the monoclinic form (r.m.s.d. = 0.9 Å), the C-terminal parts of the synaptobrevin 2 TMRs deviate slightly, indicating some conformational flexibility (see Supplementary Fig. 4a, b). In the $I2_12_12_1$ crystals, again four SNARE complexes form an X-shaped assembly, with the contacts being mainly mediated by the TMRs. However, the overall packing differs from *C*2 packing (see Supplementary Fig. 3b). Although both inter-complex contacts at the TMRs and the angle between the TMRs are likely to be determined by crystal packing, it is conceivable that such contacts have a role during the transition states of the fusion reaction.

Helical continuity throughout the linkers and TMRs is unexpected, considering that perturbation of the linkers between the SNARE motifs and the TMRs, although adversely affecting fusion, seem to be better tolerated than perturbations of the SNARE motifs, in which single point mutations can abolish function[12,22–24]. Insertion of short flexible elements between SNARE motif and TMR has only mild effects, but fusion of both biological and artificial membranes is progressively inhibited when the length of the insert is extended. Recently, synaptobrevin 2 variants carrying linker mutations were overexpressed in chromaffin cells that lack endogenous synaptobrevins and hence Ca^{2+}-regulated exocytosis[25]. Whereas wild-type synaptobrevin 2 fully rescued exocytosis, insertion of six amino acids just in front of the TMR of synaptobrevin 2 almost completely abolished fast secretion. Furthermore, although the Ca^{2+} threshold for release remained unchanged, the delay between the rise of intracellular Ca^{2+} concentration and the onset of release was increased, indicating a 'weakening' of the fusion machine operating downstream of the Ca^{2+} trigger. On the other hand, the effect of inserting two supposedly helix-breaking proline residues in the linker on exocytosis

Table 1 | Melting temperatures for all neuronal SNARE complexes

Protein constructs	*n*	Melting temperature (°C)	s.d.
Wild type	9	94.9	1.4
K256A	4	93.2	0.5
Y257A	5	90.6	0.3
Q258A	4	95.1	0.7
K260A	4	94.4	0.4
R262A	4	93.5	0.8
R263A	6	94.2	0.6
K264A	5	94.4	0.6
K265A	4	94.2	0.4
No TMR	5	84.9	0.6
Syb2 TMR	4	80.7	0.7
Sx1A TMR	5	88.6	0.6
Used in crystallization	4	96.5	0.5

For investigating the role of single amino acids in complex stability, complexes containing both TMRs and the indicated mutations in syntaxin 1A were prepared. Ellipticity at 222 nm was monitored and the inflection point of the melting transition taken to be the melting temperature.

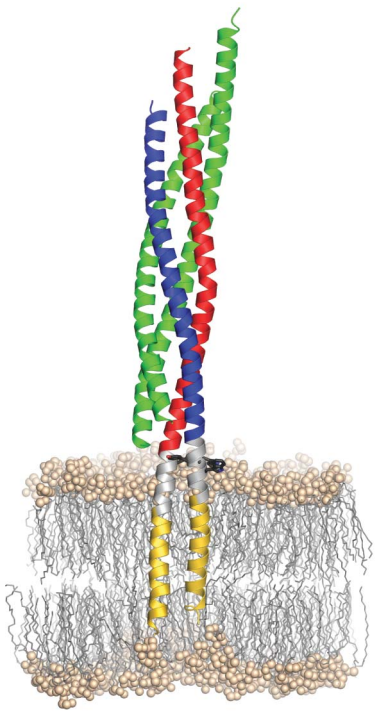

Figure 4 | Model of the synaptic SNARE complex inserted in a membrane. As a landmark, aromatic residues (black sticks) within the linker region (grey) are shown. The hydrophilic head groups of the phospholipids are shown as balls, their aliphatic chains as sticks. The position of the complex in the palmitoyl-oleoyl-phosphatidylethanolamine (POPE) bilayer was estimated from a short (54.9 ns) molecular dynamics simulation, where the apolar parts of the TMRs were initially centred within the hydrophobic part of the bilayer. Because PE head groups are highly abundant in animal membranes and PO is a relatively short tail group, POPE lipids were chosen to mimic a simple membrane with a thickness of approximately 4.5–5.0 nm.

was surprisingly mild, in agreement with an earlier study in which no serious growth defects were observed when two prolines were inserted into the linker of the yeast syntaxin homologue Sso1p[26]. However, the mild phenotypes may be at least partially explained by overexpression of the mutant proteins, because a much stronger phenotype was observed when the $(Pro)_2$-Sso1p variant was driven by the endogenous Sso1 promoter[26].

Figure 4 shows a model in which the SNARE complex was placed into a lipid bilayer. It represents the final stage of SNARE-mediated membrane fusion in which both TMRs come to rest in the same bilayer (*cis* complex). However, it raises interesting questions about the structural features of the complex before zippering is completed (*trans* complex). Although it is conceivable that in a partially zippered complex the non-assembled regions between the N-terminally assembled helical parts and the (presumably) helical transmembrane domains are unstructured, it is also possible that small helical regions exist that may provide a binding site for late regulatory proteins such as synaptotagmin and complexin. The model illustrates that the four-helix bundle of the SNARE motifs sits as a perpendicular rod directly on top of the phospholipid bilayer. With the linkers of synaptobrevin 2 and syntaxin 1A buried in the top layer of the membrane, it is difficult to imagine how the four-helix bundle can be fully zippered before membrane merger is at least initiated, but we cannot exclude that zippering is confined to SNARE complexes surrounding the neck of a fusion pore that may form only transiently (kiss-and-run mode). Accordingly, it is understandable that structural perturbations in the linkers are less disruptive for fusion and may be at least partially compensated by engaging more SNARE complexes in the fusion reaction. Our data strongly support the view that SNAREs constitute a robust and simple fusion catalyst. SNAREs operate as nanomachines in which the energy barrier of membrane fusion is overcome by the energy provided during progressive N–C zippering of the SNARE proteins all the way into the membrane.

METHODS SUMMARY

All SNARE monomers were separately expressed from pET28a as His_6-tagged proteins in *Escherichia coli* Bl21 (DE3) cells and purified by Ni^{2+}-NTA and ion exchange chromatography. SNARE complexes were then assembled from monomers and purified by ion exchange and size-exclusion chromatography. Diffraction data were collected on beamline X10SA at the Swiss Light Source of the Paul Scherrer Institut (Switzerland) and processed with HKL-2000. Initial phases were obtained from SAD data from crystals containing selenomethionine-labelled syntaxin 1A that diffracted to 4.3 Å resolution. For the final model building, native diffraction data to 3.4 Å resolution were used. Model building and refinement were performed using the programs COOT and PHENIX, respectively.

Full Methods and any associated references are available in the online version of the paper at www.nature.com/nature.

Received 26 January; accepted 15 May 2009.
Published online 1 July 2009.

1. Martens, S. & McMahon, H. T. Mechanisms of membrane fusion: disparate players and common principles. *Nature Rev. Mol. Cell Biol.* **9,** 543–556 (2008).
2. Jahn, R. & Scheller, R. H. SNAREs–engines for membrane fusion. *Nature Rev. Mol. Cell Biol.* **7,** 631–643 (2006).
3. Rizo, J. & Rosenmund, C. Synaptic vesicle fusion. *Nature Struct. Mol. Biol.* **15,** 665–674 (2008).
4. Pelham, H. R., Banfield, D. K. & Lewis, M. J. SNAREs involved in traffic through the Golgi complex. *Cold Spring Harb. Symp. Quant. Biol.* **60,** 105–111 (1995).
5. Hanson, P. I., Heuser, J. E. & Jahn, R. Neurotransmitter release — four years of SNARE complexes. *Curr. Opin. Neurobiol.* **7,** 310–315 (1997).
6. Lin, R. C. & Scheller, R. H. Structural organization of the synaptic exocytosis core complex. *Neuron* **19,** 1087–1094 (1997).
7. Sutton, R. B., Fasshauer, D., Jahn, R. & Brunger, A. T. Crystal structure of a SNARE complex involved in synaptic exocytosis at 2.4 Å resolution. *Nature* **395,** 347–353 (1998).
8. Brunger, A. T. Structure and function of SNARE and SNARE-interacting proteins. *Q. Rev. Biophys.* **38,** 1–47 (2005).
9. Kloepper, T. H., Kienle, N. C. & Fasshauer, D. An elaborate classification of SNARE proteins sheds light on the conservation of the eukaryotic endomembrane system. *Mol. Biol. Cell* **18,** 3463–3471 (2007).
10. Fasshauer, D. *et al.* A structural change occurs upon binding of syntaxin to SNAP-25. *J. Biol. Chem.* **272,** 4582–4590 (1997).
11. Fasshauer, D. *et al.* Structural changes are associated with soluble *N*-ethylmaleimide-sensitive fusion protein attachment protein receptor complex formation. *J. Biol. Chem.* **272,** 28036–28041 (1997).
12. Sorensen, J. B. *et al.* Sequential N- to C-terminal SNARE complex assembly drives priming and fusion of secretory vesicles. *EMBO J.* **25,** 955–966 (2006).
13. Pobbati, A. V., Stein, A. & Fasshauer, D. N- to C-terminal SNARE complex assembly promotes rapid membrane fusion. *Science* **313,** 673–676 (2006).
14. Su, Z., Ishitsuka, Y., Ha, T. & Shin, Y. K. The SNARE complex from yeast is partially unstructured on the membrane. *Structure* **16,** 1138–1146 (2008).
15. Dennison, S. M., Bowen, M. E., Brunger, A. T. & Lentz, B. R. Neuronal SNAREs do not trigger fusion between synthetic membranes but do promote PEG-mediated membrane fusion. *Biophys. J.* **90,** 1661–1675 (2006).
16. Jackson, M. B. & Chapman, E. R. Fusion pores and fusion machines in Ca^{2+}-triggered exocytosis. *Annu. Rev. Biophys. Biomol. Struct.* **35,** 135–160 (2006).
17. Rizo, J., Chen, X. & Arac, D. Unraveling the mechanisms of synaptotagmin and SNARE function in neurotransmitter release. *Trends Cell Biol.* **16,** 339–350 (2006).
18. Fasshauer, D., Antonin, W., Subramaniam, V. & Jahn, R. SNARE assembly and disassembly exhibit a pronounced hysteresis. *Nature Struct. Biol.* **9,** 144–151 (2002).
19. Poirier, M. A. *et al.* Protease resistance of syntaxin·SNAP-25·VAMP complexes. Implications for assembly and structure. *J. Biol. Chem.* **273,** 11370–11377 (1998).
20. Ernst, J. A. & Brunger, A. T. High resolution structure, stability, and synaptotagmin binding of a truncated neuronal SNARE complex. *J. Biol. Chem.* **278,** 8630–8636 (2003).
21. Lam, A. D. *et al.* SNARE-catalyzed fusion events are regulated by syntaxin1A–lipid interactions. *Mol. Biol. Cell* **19,** 485–497 (2008).
22. McNew, J. A. *et al.* The length of the flexible SNAREpin juxtamembrane region is a critical determinant of SNARE-dependent fusion. *Mol. Cell* **4,** 415–421 (1999).
23. Wang, Y., Dulubova, I., Rizo, J. & Sudhof, T. C. Functional analysis of conserved structural elements in yeast syntaxin Vam3p. *J. Biol. Chem.* **276,** 28598–28605 (2001).
24. Deak, F., Shin, O. H., Kavalali, E. T. & Sudhof, T. C. Structural determinants of synaptobrevin 2 function in synaptic vesicle fusion. *J. Neurosci.* **26,** 6668–6676 (2006).
25. Kesavan, J., Borisovska, M. & Bruns, D. v-SNARE actions during Ca^{2+}-triggered exocytosis. *Cell* **131,** 351–363 (2007).
26. Van Komen, J. S. *et al.* The polybasic juxtamembrane region of Sso1p is required for SNARE function *in vivo*. *Eukaryot. Cell* **4,** 2017–2028 (2005).
27. Fasshauer, D., Sutton, R. B., Brunger, A. T. & Jahn, R. Conserved structural features of the synaptic fusion complex: SNARE proteins reclassified as Q- and R-SNAREs. *Proc. Natl Acad. Sci. USA* **95,** 15781–15786 (1998).

Supplementary Information is linked to the online version of the paper at www.nature.com/nature.

Acknowledgements We thank U. Ries for technical assistance, C. Kutzner and H. Grubmüller for providing the model shown in Fig. 4, R. Lührmann for access to his X-ray facilities, D. Fasshauer and N. Pavlos for comments on the manuscript, W. Antonin for providing the expression constructs of endosomal SNAREs and the staff of beamlines PX1 and PX2 of the Swiss Light Source for support during diffraction data collection.

Author Contributions A.S. and R.J. planned the project, A.S. performed the experiments, A.S., G.W. and M.C.W. analysed the data and A.S. and R.J. wrote the manuscript. All authors discussed the results and commented on the manuscript.

Author Information Reprints and permissions information is available at www.nature.com/reprints. Correspondence and requests for materials should be addressed to R.J. (rjahn@gwdg.de).

METHODS

Protein constructs. The SNARE proteins syntaxin 1A, 7 and 8, SNAP-25A, synaptobrevin 2 and endobrevin from rat and Vti1b from mouse were used. The following expression constructs (all in pET28a) have been described: syntaxin 1A (residues 180–262 and 183–288)[28,29], syntaxin 7 (residues 159–236), syntaxin 8 (residues 136–213), SNAP-25A (residues 7–83, 141–204 and a full-length version in which all cysteines were mutated to serines)[30,31], synaptobrevin 2 (residues 1–96 and 1–116)[28,29], Vti1b (residues 130–206) and endobrevin (residues 1–74 and 1–100)[31–33]. For crystallization of the neuronal SNARE complex, DNA encoding a synaptobrevin 2 fragment lacking the N-terminal proline-rich region was cloned into pET28a via NdeI/XhoI restriction sites (residues 30–116). Genes of the endosomal SNAREs containing TMRs were also cloned into pET28a via NdeI/XhoI restriction sites: syntaxin 7 (residues 159–261), syntaxin 8 (residues 136–236), Vti1b (residues 130–232).

Protein expression and purification. Protein purification was carried out essentially as described[13,29,30,32,34]. Briefly, all proteins were expressed in *E. coli* strain BL21 (DE3) and purified by Ni^{2+}-NTA affinity chromatography followed by ion exchange chromatography on an Äkta system (GE Healthcare). Syntaxin 1A (residues 183–288) and syntaxin 7 (residues 159–261) were desalted after Ni^{2+}-NTA affinity chromatography and removal of their tags on a HiPrep 26/10 Desalting column (GE Healthcare) equilibrated with 20 mM Tris buffer pH 8.8, 500 mM NaCl, 50 mM *n*-octyl β-D-glucopyranoside, 1 mM tris-(2-carboxyethyl) phosphine (TCEP) without further purification by ion-exchange chromatography. Synaptobrevin 2 (residues 1–116 and 30–116) and all endosomal SNAREs containing TMRs were purified by ion exchange chromatography in the presence of 50 mM *n*-octyl β-D-glucopyranoside. Selenomethionine-labelled syntaxin 1A was expressed in minimal medium containing selenomethionine as described[35]. Purification was performed in the presence of 10 mM β-mercaptoethanol during Ni^{2+}-NTA affinity chromatography, and 10 mM dithiothreitol in all subsequent steps. All SNARE complexes were assembled by overnight incubation of the monomers at 4 °C, using syntaxin 1A or syntaxin 7 as the limiting components. Complexes were then separated from free monomers by ion-exchange chromatography in the presence of 50 mM *n*-octyl β-D-glucopyranoside (neuronal complexes used for CD experiments), 12 mM *n*-nonyl β-D-glucopyranoside, 140 mM *n*-heptyl β-D-glucopyranoside (complexes used for crystallization) or 0.03% (w/v) *n*-dodecyl β-D-maltopyranoside (endosomal complex). Complexes used for crystallization were additionally purified by size-exclusion chromatography using a Superdex 200 column equilibrated with 10 mM Tris, pH 8.8, 1 M NaCl, 1 mM TCEP and 12 mM *n*-nonyl β-D-glucopyranoside or 140 mM *n*-heptyl β-D-glucopyranoside.

Crystallization and data collection. For crystallization, the neuronal SNARE complex was reconstituted from the following monomers: syntaxin 1A (residues 183–288), SNAP-25A (residues 7–83 and 141–204) and synaptobrevin 2 (residues 30–116). Initial crystals diffracting to about 8 Å resolution were obtained using *n*-octyl β-D-glucopyranoside as a stabilizing detergent. Variation of the length of the aliphatic chain by ±1 methylene group yielded crystals that diffracted to about 4.8 and 4.3 Å for *n*-heptyl β-D-glucopyranoside and *n*-nonyl β-D-glucopyranoside, respectively. The complex purified in the presence of *n*-nonyl β-D-glucopyranoside crystallized in sitting drops at 20 °C. Crystals were obtained by mixing protein at a concentration of 15–20 mg ml^{-1} in a 1:1 ratio with reservoir solution containing 100 mM HEPES, pH 7.3, 200 mM Li_2SO_4, 100 mM NaCl, 29% PEG 400 and 30 mM Gly-Gly-Gly. Crystals appeared after 2–3 days and grew within 2 weeks to about 0.1–0.3 mm in each dimension. Before freezing, single crystals were transferred to a 5 µl drop of 100 mM HEPES, pH 7.3, 200 mM Li_2SO_4, 100 mM NaCl, 35% PEG 400, 30 mM Gly-Gly-Gly, 12 mM *n*-nonyl β-D-glucopyranoside and placed on ice for 1–3 h. Crystals were then flash-frozen in a 100 K nitrogen stream. This procedure improved diffraction to a minimum Bragg spacing of 3.4 Å.

For the crystallization of the complex purified in the presence of *n*-heptyl β-D-glucopyranoside, the reservoir solution contained 100 mM Tris, pH 8.8, 50 mM $MgCl_2$, 16% 2-methyl-2,4-pentanediol and 3% (w/v) sorbitol. These crystals were cryo-protected by transfer into perfluoropolyether and then flash-frozen in liquid nitrogen. Data sets were collected on frozen crystals at 100 K on the X10SA beamline at the Swiss Light Source of the Paul Scherrer Institut (Switzerland) using a MAR225 CCD detector. The data were indexed, integrated and scaled with the HKL-2000 package[36] (Supplementary Table 1).

Structure determination. The crystals obtained with *n*-nonyl β-D-glucopyranoside belong to space group *C*2 ($a = 265.4$ Å, $b = 135.5$ Å, $c = 58.7$ Å, $\beta = 96.3°$) with two complexes and 82% solvent in the crystallographic asymmetric unit. Initial experimental phases were obtained by SAD phasing using a complex with selenomethionine-labelled syntaxin 1A, which was crystallized and diffracted to a resolution of 4.3 Å. Using the SHELX package[37] 12 out of 14 methionines present in a crystallographic asymmetric unit were located. An initial model was generated by placing a high-resolution structure of the neuronal core complex[20] into the experimental electron density using MOLREP[38] and manually extending the structure into the linkers and TMRs with COOT[39]. This model was transferred to a 3.4 Å native data set and further refined by manual model building and automated refinement with REFMAC5[40] including TLS (translation, liberation and screw-rotation) refinement[41]. Final refinement was performed using the PHENIX.REFINE program[42]. During all refinement cycles, non-crystallographic symmetry restraints were imposed on the structures of the two crystallographically independent complexes. The positions of methionines in syntaxin 1A, including one methionine in the TMR, were subsequently verified using the anomalous difference density from the selenomethionine data set.

The structure in the orthorhombic form was solved by molecular replacement using the structure obtained for the monoclinic form as a search model. The shift in the TMR was clearly observed as difference electron density in the $F_o - F_c$ map and corrected by manual model building followed by automated refinement using the PHENIX.REFINE program, imposing strong restraints on the non-crystallographic symmetry and geometry, and refining one B factor per amino acid[42]. TLS refinement did not lead to a considerable improvement of *R*-factors and was therefore not performed.

CD spectroscopy. CD measurements were performed using a Chirascan instrument (Applied Photophysics). Hellma quartz cuvettes with a path length of 0.1 cm were used. For thermal denaturation experiments, complexes were dissolved to 5 µM in 20 mM sodium phosphate, pH 7.4, 500 mM NaF, 0.1 mM TCEP, 34 mM *n*-octyl β-D-glucopyranoside. The ellipticity at 222 nm was recorded between 20 and 100 °C with a temperature increment of 15 °C h^{-1} for the neuronal complexes, and 30 °C h^{-1} for the endosomal complexes. The temperature was measured with a temperature probe placed in the solution. For chemical denaturation experiments, complexes were dissolved to 3 µM in 20 mM sodium phosphate, 0.02% *n*-dodecyl β-D-maltopyranoside and the indicated amounts of GndHCl. After at least 8 h incubation in the respective buffer, far-ultraviolet CD spectra were recorded at 20 °C using steps of 0.2 nm with an averaging time of 1 s. For data analysis, ellipticity recorded at 222 nm was converted to fraction of unfolded protein. In the case of the neuronal complex with both TMRs, total unfolding was not achieved at 20 °C and approximately 6.5 M GndHCl. The solution was therefore heated to 95 °C and the corresponding ellipticity at 222 nm used for normalization. For the other complexes this procedure did not result in any further change in ellipticity.

Molecular dynamics simulation. Individual lipids (229) were taken from an equilibrated POPE membrane simulation and subsequently placed around the complex such that the average area per lipid molecule was that of the donor membrane. The remaining unoccupied volume of the simulation box was then filled with 26,629 SPC/E (simple point charge/extended) water molecules[43]. For the SNARE complex the optimized potentials for liquid simulations all-atom force field was used[44] and lipid parameters were taken from ref. 45. After energy-minimizing the SNARE complex, water and membrane were separately equilibrated for 10 ps each. For the subsequent simulation the protein was kept as a rigid body, whereas phospholipids and water were allowed to move freely. The simulation was performed with GROMACS 4.0.3 (ref. 46). Cutoffs were set to 1.0 nm, long-range electrostatics were calculated with the particle-mesh Ewald method. Berendsen temperature and pressure coupling was used to keep the system at 300 K and 1 bar[47]. Using a time step length of 2 fs, the LINCS and SETTLE constraint algorithms were applied[48,49].

28. Fasshauer, D., Eliason, W. K., Brunger, A. T. & Jahn, R. Identification of a minimal core of the synaptic SNARE complex sufficient for reversible assembly and disassembly. *Biochemistry* **37,** 10354–10362 (1998).
29. Schuette, C. G. *et al.* Determinants of liposome fusion mediated by synaptic SNARE proteins. *Proc. Natl Acad. Sci. USA* **101,** 2858–2863 (2004).
30. Pobbati, A. V. *et al.* Structural basis for the inhibitory role of tomosyn in exocytosis. *J. Biol. Chem.* **279,** 47192–47200 (2004).
31. Fasshauer, D. *et al.* Mixed and non-cognate SNARE complexes. Characterization of assembly and biophysical properties. *J. Biol. Chem.* **274,** 15440–15446 (1999).
32. Antonin, W. *et al.* A SNARE complex mediating fusion of late endosomes defines conserved properties of SNARE structure and function. *EMBO J.* **19,** 6453–6464 (2000).
33. Brandhorst, D. *et al.* Homotypic fusion of early endosomes: SNAREs do not determine fusion specificity. *Proc. Natl Acad. Sci. USA* **103,** 2701–2706 (2006).
34. Stein, A. *et al.* Synaptotagmin activates membrane fusion through a Ca^{2+}-dependent *trans* interaction with phospholipids. *Nature Struct. Mol. Biol.* **14,** 904–911 (2007).
35. Van Duyne, G. D. *et al.* Atomic structures of the human immunophilin FKBP-12 complexes with FK506 and rapamycin. *J. Mol. Biol.* **229,** 105–124 (1993).
36. Otwinowski, Z. & Minor, W. Processing of X-ray diffraction data collected in the oscillation mode. *Methods Enzymol.* **276,** 307–326 (1997).
37. Sheldrick, G. M. A short history of SHELX. *Acta Crystallogr. A* **64,** 112–122 (2008).
38. Vagin, A. & Teplyakov, A. An approach to multi-copy search in molecular replacement. *Acta Crystallogr. D* **56,** 1622–1624 (2000).

39. Emsley, P. & Cowtan, K. *Coot*: model-building tools for molecular graphics. *Acta Crystallogr. D* **60,** 2126–2132 (2004).
40. Murshudov, G. N., Vagin, A. A. & Dodson, E. J. Refinement of macromolecular structures by the maximum-likelihood method. *Acta Crystallogr. D* **53,** 240–255 (1997).
41. Winn, M. D., Isupov, M. N. & Murshudov, G. N. Use of TLS parameters to model anisotropic displacements in macromolecular refinement. *Acta Crystallogr. D* **57,** 122–133 (2001).
42. Adams, P. D. *et al. PHENIX*: building new software for automated crystallographic structure determination. *Acta Crystallogr. D* **58,** 1948–1954 (2002).
43. Berendsen, H. J. C., Grigera, J. R. & Straatsma, T. P. The missing term in effective pair potentials. *J. Phys. Chem.* **91,** 6269–6271 (1987).
44. Kaminski, G. A., Friesner, R. A., Tirado-Rives, J. & Jorgensen, W. L. Evaluation and reparametrization of the OPLS-AA force field for proteins via comparison with accurate quantum chemical calculations on peptides. *J. Phys. Chem. B* **105,** 6474–6487 (2001).
45. Berger, O., Edholm, O. & Jahnig, F. Molecular dynamics simulations of a fluid bilayer of dipalmitoylphosphatidylcholine at full hydration, constant pressure, and constant temperature. *Biophys. J.* **72,** 2002–2013 (1997).
46. Hess, B., Kutzner, C., van der Spoel, D. & Lindahl, E. GROMACS 4: Algorithms for highly efficient, load-balanced, and scalable molecular simulation. *J. Chem. Theory Comput.* **4,** 435–447 (2008).
47. Berendsen, H. J. C. *et al.* Molecular dynamics with coupling to an external bath. *J. Chem. Phys.* **81,** 3684–3690 (1984).
48. Hess, B. P-LINCS: A parallel linear constraint solver for molecular simulation. *J. Chem. Theory Comput.* **4,** 116–122 (2008).
49. Miyamoto, S. & Kollman, P. A. SETTLE: an analytical version of the SHAKE and RATTLE algorithm for rigid water models. *J. Comput. Chem.* **13,** 952–962 (1992).